Aging rate of spin glasses from simulations matches experiments

M. Baity-Jesi,[1, 2] E. Calore,[3] A. Cruz,[4, 2] L.A. Fernandez,[5, 2] J.M. Gil-Narvion,[2] A. Gordillo-Guerrero,[6, 7, 2]
D. Iñiguez,[2, 8] A. Maiorano,[9, 2] E. Marinari,[10] V. Martin-Mayor,[5, 2] J. Moreno-Gordo,[2, 4]
A. Muñoz-Sudupe,[5, 2] D. Navarro,[11] G. Parisi,[10] S. Perez-Gaviro,[12, 2, 4] F. Ricci-Tersenghi,[10]
J.J. Ruiz-Lorenzo,[13, 7, 2] S.F. Schifano,[14] B. Seoane,[15, 2] A. Tarancon,[4, 2] R. Tripiccione,[3] and D. Yllanes[16, 2, *]

(Janus Collaboration)

[1]*Department of Chemistry, Columbia University, New York, NY 10027, USA*
[2]*Instituto de Biocomputación y Física de Sistemas Complejos (BIFI), 50018 Zaragoza, Spain*
[3]*Dipartimento di Fisica e Scienze della Terra, Università di Ferrara e INFN, Sezione di Ferrara, I-44122 Ferrara, Italy*
[4]*Departamento de Física Teórica, Universidad de Zaragoza, 50009 Zaragoza, Spain*
[5]*Departamento de Física Teórica, Universidad Complutense, 28040 Madrid, Spain*
[6]*Departamento de Ingeniería Eléctrica, Electrónica y Automática, U. de Extremadura, 10003, Cáceres, Spain*
[7]*Instituto de Computación Científica Avanzada (ICCAEx),*
Universidad de Extremadura, 06006 Badajoz, Spain
[8]*Fundación ARAID, Diputación General de Aragón, Zaragoza, Spain*
[9]*Dipartimento di Fisica, Sapienza Università di Roma, I-00185 Rome, Italy*
[10]*Dipartimento di Fisica, Sapienza Università di Roma, INFN,*
Sezione di Roma 1, and CNR-Nanotec, I-00185 Rome, Italy
[11]*Departamento de Ingeniería, Electrónica y Comunicaciones and I3A, U. de Zaragoza, 50018 Zaragoza, Spain*
[12]*Centro Universitario de la Defensa, Carretera de Huesca s/n, 50090 Zaragoza, Spain*
[13]*Departamento de Física, Universidad de Extremadura, 06006 Badajoz, Spain*
[14]*Dipartimento di Matematica e Informatica, Università di Ferrara e INFN, Sezione di Ferrara, I-44122 Ferrara, Italy*
[15]*Laboratoire de physique théorique, Département de physique de l'ENS,*
École normale supérieure, PSL Research University,
Sorbonne Université, CNRS, 75005 Paris, France
[16]*Department of Physics and Soft and Living Matter Program, Syracuse University, Syracuse, NY, 13244*
(Dated: August 15, 2018)

Experiments on spin glasses can now make precise measurements of the exponent $z(T)$ governing the growth of glassy domains, while our computational capabilities allow us to make quantitative predictions for experimental scales. However, experimental and numerical values for $z(T)$ have differed. We use new simulations on the Janus II computer to resolve this discrepancy, finding a time-dependent $z(T, t_\mathrm{w})$, which leads to the experimental value through mild extrapolations. Furthermore, theoretical insight is gained by studying a crossover between the $T = T_\mathrm{c}$ and $T = 0$ fixed points.

The study of spin glasses (SGs) [1, 2] has long been a key problem in statistical mechanics, providing ideas that have born fruit in fields as diverse as econophysics, biology or optimization in computer science. From a fundamental point of view, SGs are paradigmatic as the most approachable model for glassy behavior, both experimentally and theoretically. However, despite this relative simplicity, SG experiments and theory have traditionally developed separately, for practical and conceptual reasons. On the one hand, numerical simulations were not long enough to reach experimental times, while experiments were not precise enough or even able to measure key physical quantities. On the other hand, experimental samples are perennially out of equilibrium, while theory mostly focuses on the (unreachable) equilibrium phase.

In a typical experiment, the system is rapidly cooled to a subcritical working temperature $T < T_\mathrm{c}$ and its off-equilibrium evolution (aging) studied. As the waiting time t_w increases, the size of the glassy domains is seen to grow as $\xi(t_\mathrm{w}) \propto t_\mathrm{w}^{1/z(T)}$, with an exponent that is expected to behave as $z(T) \simeq z(T_\mathrm{c})T_\mathrm{c}/T$ [3]. In traditional experiments [4], based on the shift of the peak in the relaxation rate $S(t_\mathrm{w})$, $z(T)$ was difficult to measure. Fortunately, the availability of excellent samples with a film geometry has suggested a new approach to the precision measurement of $z_\mathrm{c} = z(T)T/T_\mathrm{c}$ [5]. The time that $\xi(t_\mathrm{w})$ needs to saturate to the film thickness relates to the activation energies Δ_max [6, 7]. Varying the film thickness from 9 to 20 nm resulted in the measurement $z_\mathrm{c} \approx 9.62$ [5], very far from the value predicted by numerical simulations $z_\mathrm{c} = 6.86(16)$ [8], $z_\mathrm{c} = 6.80(15)$ [9].

Fortunately, recent theoretical progress makes it feasible to address the above-mentioned disagreement. A key development has been the introduction of the Janus [10, 11] and Janus II [12] computers, which have extended the numerical exploration of the dynamics almost to the experimental scale [8, 13]. In addition, the introduction of quantitative statics-dynamics dictionaries (first based on microscopic quantities [8, 14, 15] and more recently on experimentally measurable features [13]) has clarified the relevance of the equilibrium phase for the off-equilibrium

dynamics and showed how to extrapolate simulations to the experimental scale. Finally, the (macroscopic) experimental measurement of the size of glassy domains was shown to be consistent with the (microscopic) definition based on correlation functions [16].

Here we resolve the discrepancy in z_c by finding a (very mild) scale dependence in the dynamical exponent $z(T, \xi(t_w))$. We first recognize that *time* should be traded by *length* scales. Gentle extrapolations to the relevant experimental scales of 20 nm [5] then reconcile the numerical and experimental measurements. Such a computation has been possible only thanks to new data with unprecedented precision, achieved by reducing the uncertainty due to thermal fluctuations, an issue that was typically neglected in previous numerical work. From the theoretical point of view, our study is based on a characterization of the crossover between critical and low-temperature behavior. This is a very important point, since it resolves a theoretical controversy on how low a temperature must be studied to be free of critical effects, with some authors choosing to work at very low T at the expense of the system sizes that it is possible to equilibrate (e.g., [17]) and others trying to find a tradeoff between temperature and system size (e.g., [14]).

We consider the standard Edwards-Anderson model [18], defined on a three-dimensional cubic lattice of side $L = 160$, on whose nodes we place spins $S_x = \pm 1$ that interact with their lattice nearest neighbors through

$$\mathcal{H} = - \sum_{\langle x,y \rangle} J_{xy} S_x S_y . \qquad (1)$$

For each disorder realization $\{J_{xy}\}$ (a sample), each of the quenched couplings J_{xy} is ± 1 with 50% probability. We shall refer to thin CuMn films [5], where the film thickness of 20 nm translates to a distance of 38 lattice spacings (the typical Mn-Mn distance is 5.3Å).

Our systems are initialized with random orientations for the spins (representing a very high starting temperature) and immediately quenched to the working temperature $T < T_c = 1.102(3)$ [19]. We then follow the evolution with the waiting time t_w (measured in units of full lattice sweeps) at constant temperature. For each sample $\{J_{xy}\}$ we simulate N_R real replicas, evolving with different thermal noise. We estimate our statistical errors with a jackknife method [20] (including fit parameters [21]).

Our basic observable is the spatial autocorrelation of the overlap field (discussed in detail in [22]),

$$C_4(T, \boldsymbol{r}, t_w) = \overline{\langle q^{(a,b)}(\boldsymbol{x}, t_w) q^{(a,b)}(\boldsymbol{x} + \boldsymbol{r}, t_w) \rangle_T}, \qquad (2)$$

$$q^{(a,b)}(\boldsymbol{x}, t_w) = S^{(a)}(\boldsymbol{x}, t_w) S^{(b)}(\boldsymbol{x}, t_w). \qquad (3)$$

In these equations, the indices (a, b) label the different real replicas; $\langle \cdots \rangle_T$ is the average over the thermal noise [in practice, an average over the (a, b) pairs] and $\overline{(\cdots)}$ is the average over the disorder. In equilibrium simulations, by far the main source of error are the sample-to-sample
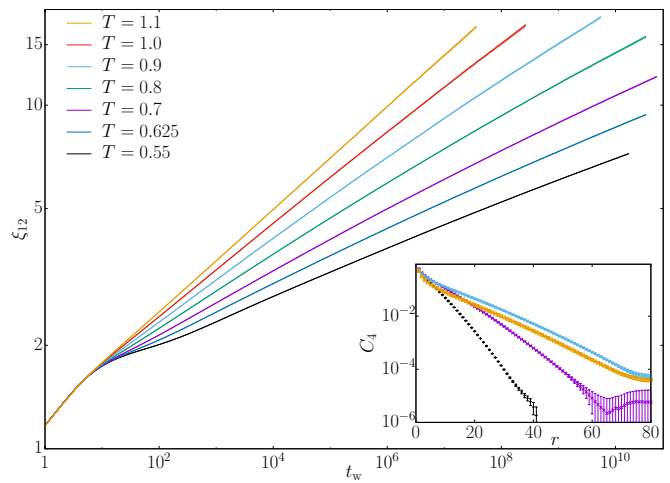

FIG. 1. Growth of the coherence length $\xi_{12}(T, t_w)$ with the waiting time t_w after a quench to temperature T in a log-log scale [the critical temperature is $T_c = 1.102(3)$]. Given the smallness of the statistical errors, instead of error bars we have plotted two lines for each T, which enclose the error estimate. At this scale, the curves seem linear for long times, indicating a power-law growth but, see Fig. 2, there is actually a measurable curvature. *Inset:* Spatial autocorrelation function of the overlap field $C_4(T, r, t_w)$, plotted as a function of distance at the last simulated time for several temperatures. Note the six orders of magnitude in the vertical axis.

fluctuations. Therefore, it has been customary to simulate the smallest N_R that permits definitions such as (2) and maximize the number N_S of samples. Instead, we have $N_R = 256$ and $N_S = 16$. This choice, motivated to facilitate future studies of temperature chaos [23], has proven crucial: contrary to our expectations, the increase in N_R has produced a dramatic reduction of statistical errors (see Appendix A for details). As a result, we have been able to follow the decay of $C_4(T, r, t_w)$ over six decades (see inset to Fig. 1). A similar dramatic error reduction with high N_R has also been seen in studies of the Gardner transition in structural glasses [24, 25].

These correlation functions decay with distance as

$$C_4(T, r, t_w) = r^{-\theta} f(r/\xi(T, t_w)), \qquad (4)$$

so the growing ξ can be computed through integral estimators [8, 22]: $I_k(T, t_w) = \int_0^\infty dr \; r^k C_4(T, r, t_w)$. Then $\xi_{k,k+1}(T, t_w) = I_{k+1}(T, t_w)/I_k(T, t_w)$. As in recent work [13, 16, 22, 26] we use $k = 1$ (see [27] for technical details). The resulting ξ_{12} is plotted in Fig. 1 for all our working temperatures.

The numerical [8, 22, 26] and experimental [5] state of the art describes the growth of ξ_{12} with a power law,

$$\xi_{12}(T, t_w) \simeq A(T) \, t_w^{1/z(T)} . \qquad (5)$$

However, with our increased precision, (5) is no longer a faithful representation of the dynamics. Indeed, if we switch to $x = \log \xi_{12}$ as independent variable we can interpolate our data as

$$\log t_w(T, \xi_{12}) = c_0(T) + c_1(T) \, x + c_2(T) \, x^2. \qquad (6)$$
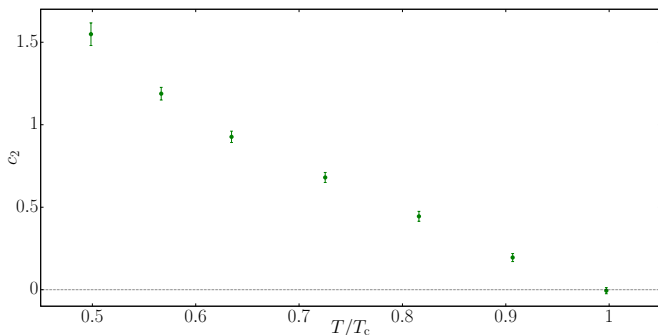
FIG. 2. Deviation of $\xi_{12}(t_w)$ from a simple power-law growth. We plot the quadratic parameter c_2 in a fit to (6) (see Appendix D for fitting parameters). This quantity is zero at the critical point, but has a positive value at low temperatures, indicating that the growth of ξ_{12} slows down over the simulated time range.

Notice that $c_2 = 0$ would reduce to (5), while $c_2 > 0$ would indicate a slowing down of the dynamics for increasing ξ_{12}. Indeed, see Fig. 2, we find that c_2 vanishes only at $T = T_c$, with $z_c = z(T = T_c) = 6.69(6)$ [28]. Of course, (6), useful as an interpolation, is not suitable to extrapolate for longer times than simulated. In order to do that, we need some insight from theory [29].

We can gain much insight into the SG phase by considering the algebraic prefactor in (4), determined by an exponent θ. At T_c, $\theta = 1 + \eta$, where $\eta = -0.390(4)$ [19] is the anomalous dimension. In the SG phase, there are differing expectations for θ in the two main theoretical pictures. The droplet description [30–32] expects coarsening domains and therefore $\theta = 0$. On the other hand, the replica symmetry breaking (RSB) theory expects space-filling domains where C_4 vanishes at constant r/ξ_{12} as t_w grows. In particular, θ is given by the replicon, a critical mode analogous to magnons in Heisenberg ferromagnets (see [15] for a detailed discussion). The best previous numerical study of θ [22], found $\theta = 0.38(2)$, with a small T dependence that was vaguely attributed to the effect of the critical point.

We can obtain θ by noticing that $I_2(T, \xi_{12}) \propto \xi_{12}^{3-\theta}$. However, again we find that, while $\theta(T_c)$ is compatible with $1 + \eta$, for $T < T_c$ we actually have $\theta(T, \xi_{12})$, slowly decreasing as ξ_{12} increases (or T decreases). This may seem an unsatisfactory result, since, in the large-ξ_{12} limit, $\theta(T, \xi_{12})$ should tend to a T-independent constant (possibly zero). The simplest explanation is that low values of ξ_{12} are affected by the $T = T_c$ fixed point with $\theta \approx 0.61$ [an idea supported by the higher measured $\theta(T, \xi_{12})$ for the higher T], while for $\xi_{12} \to \infty$ we should see a crossover to the $T = 0$ fixed point, with an unknown $\theta(T = 0)$ (see also [26]).

In analogy with the ferromagnetic phase of the $O(N)$ model, we can model this crossover in terms of a Josephson length ℓ_J [33]. Close to T_c, this should grow as $\ell_J \propto (T_c - T)^{-\nu}$, with $\nu = 2.56(4)$ [19], while scaling corrections are expected for the lowest temperatures [34].
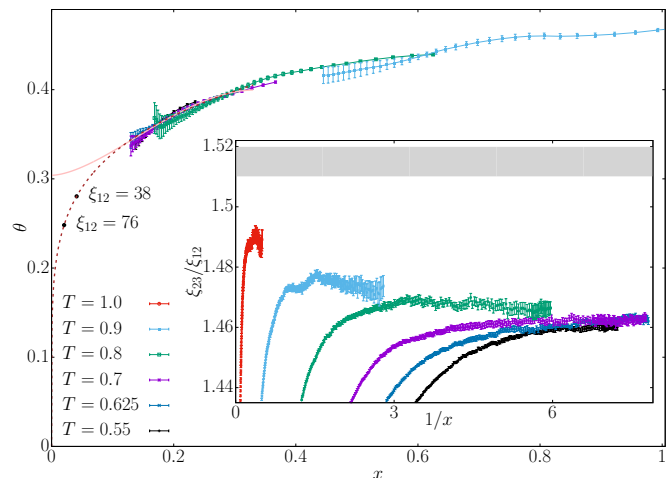

FIG. 3. Crossover between the $T = T_c$ and the $T = 0$ fixed points controlled by a Josephson length $\ell_J(T)$, with $\ell_J(T) \propto (T_c - T)^{-\nu}$ close to T_c (see text). The relevant scaling variable is $x = \ell_J(T)/\xi_{12}$. The *inset* considers the ratio ξ_{23}/ξ_{12} between two definitions of the coherence length, which should be constant in the large-ξ_{12} (or $x \to 0$) limit. For T close to T_c, this ratio initially grows, approaching the $T = T_c$ value (represented by the thick gray line) and eventually relaxes towards the $T = 0$ fixed point. *Main plot:* Evolution of the replicon exponent θ for several temperatures. We show two possible extrapolations to infinite ξ_{12}: one with finite θ, as expected in the RSB picture, and one with $\theta = 0$, as expected in the droplet picture. For the latter, we also show the extrapolated value for the experimental scale corresponding to experiments in CuMn films [5], which we estimate between $\xi_{12} = 38$ and $\xi_{12} = 76$.

If this hypothesis is correct, our data for different temperatures should come together when plotted in terms of a scaling variable $x = \ell_J/\xi_{12}$. We test this scaling in the inset to Fig. 3, where we consider the ratio ξ_{23}/ξ_{12} between two different determinations of the coherence length, which should be scale invariant in the large-ξ_{12} limit (different definitions of ξ all grow at the same rate, but differ in a small constant factor, see Fig. 4 in [22]). As expected, there is an enveloping curve for the data at different T. In particular, the curves for $T = 0.55, 0.625, 0.7$ appear free from the influence of the critical point.

Similarly, $\theta(T, \xi_{12}) = 3 - d \log I_2/d \log \xi_{12}$, which we can compute numerically (see Appendix C), turns out to be a function of x, see the collapsing curve Fig. 3. We are interested in estimating $\theta(x)$ at the experimentally relevant scale of $\xi_{\text{films}} = 38$ for thin films, recall our discussion of (1). As discussed, the RSB and droplet pictures have diverging expectations for $\theta(0)$, that is, for the $\xi_{12} \to \infty$ limit, so we can use them as upper and lower bounds. In the RSB theory, see Appendix C and Fig. 3, we can compute an extrapolation to $\theta(0) \approx 0.30$, although we take $\theta^{\text{upper}} = 0.35$ as our upper bound for θ. In the droplet description, we expect $\theta(x) = Cx^\zeta$, where ζ is in principle the stiffness exponent $\zeta \approx 0.24$ [35]. As in [14], we find that the droplet behavior can be reached
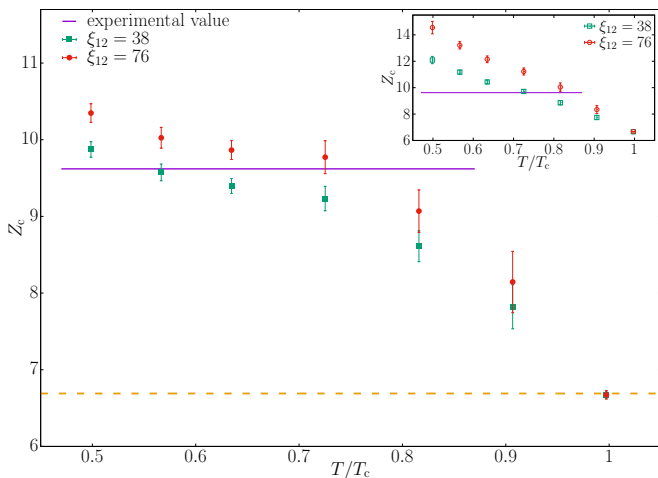
FIG. 4. Value of the experimental aging rate for SGs $Z_c(T) = z(T, \xi_{\text{films}})T/T_c$, extrapolated from our data for values of the coherence length corresponding to thin CuMn films. The main plot considers an ansatz (7) with a finite $z(T, \xi_{12} \to \infty)$, which agrees very well with the experimental value of $Z_c(T) \approx 9.62$ [5], indicated by the straight line, whose width represents the experimental temperature range. Notice that critical effects are only visible for $T > 0.7$. *Inset:* Same plot but now considering a crossover to activated dynamics (8), as in [36]. This is less successful at reproducing the roughly constant $Z_c(T)$ observed in experiments.

in the infinite-ξ_{12} limit, but only with a smaller exponent $\zeta \approx 0.15$, which, furthermore, is highly sensitive to the fitting range. Using the droplet extrapolation for $\xi_{\text{films}} = 38$ we obtain $\theta(\xi_{\text{films}}) \approx 0.28$. Since our microscopically determined ξ_{12} may differ by a small constant factor from a macroscopic measurement of ξ [16] we have also considered $\xi_{\text{films}} = 76$, which brings the exponent down to $\theta(\xi_{\text{films}}) = 0.25$ (see Fig. 3). In short, as observed in previous work [14, 15], for the experimentally relevant scale the physics is well described by a non-coarsening picture, with $0.25 < \theta(\xi_{\text{films}}) < 0.35$ depending on the theory we use to extrapolate the data and the exact value chosen for the experimental scale.

As discussed in the introduction, experiments observe a constant $z(T)T/T_c \approx 9.62$ [5]. In the previous discussion, on the other hand, we have found $z_c = 6.69(6)$ and a growing $z(T, \xi_{12})$. Therefore, in order to compare our results with experiments, the first step is finding some way to extrapolate for $\xi_{12} = \xi_{\text{films}}$. The most natural possibility, given the smoothness of the data in Fig. 1, is to assume that $t_w = A(T)\xi_{12}^{z(T,\xi_{12})}$, with a $z(T, \xi_{12})$ that tends to a finite $z_\infty(T)$ when $\xi_{12} \to \infty$, $z(T, \xi_{12}) - z_\infty(T) \propto \xi_{12}^{-\omega}$, thus

$$\log t_w = D(T) + z_\infty(T) \log \xi_{12} + E(T)\xi_{12}^{-\omega}, \quad (7)$$

where ω is the exponent that controls finite-$\xi_{12}(t_w)$ corrections. At T_c, we expect $\omega = 1.12(10)$ [9, 19, 26]. For $T < T_c$, the leading behavior is given by $\omega = \theta$ ([15] and section 4.2 in [14]). When fitting to (7), in principle one

must consider possible systematic effects from the fitting range $\xi_{12} \geq \xi_{12}^{\min}$ and the increased statistical error due to our uncertainty in the value of θ. However, see Appendix D, these effects have little impact on our final estimates.

An alternative interpretation is to consider a crossover to activated dynamics, as proposed by the Saclay group [36, 37]. Free-energy barriers are considered from a dynamical point of view, with a growth exponent Ψ,

$$\log t_w = F(T) + z_c \log \xi_{12} + G(T)\xi_{12}^\Psi, \quad (8)$$

hence $z(T, \xi_{12}) = \mathrm{d}\log t_w/\mathrm{d}\log \xi_{12} = z_c + G(T)\Psi\xi_{12}^\Psi$. Eq. (8) is a refinement of droplet theory [32] and has been used before in experiments [38] and simulations [39] with values of $\Psi \approx 1$ [40]. RSB theory is neutral with respect to choosing ansatze (7) or (8). We recall the numerical result in infinite dimensions [41] of $\tau \sim \exp(-N^b)$ for the time scales associated with the largest energy barriers, with $b \approx 1/3$ (see also [42, 43]). This result can be connected with finite D at the upper critical dimensions $D_u = 6$, which yields $\Psi(D_u) = 6b$. We note, in particular, that (7) can be regarded as a $\Psi \to 0$ limit of (8). With previous data it was not possible to distinguish the behavior of (8) and that of a simple power law [22]. With the present simulations, we find that (8) also yields good fits for $t_w(\xi_{12})$, with $\Psi \approx 0.4$ (again, the dependence on the fitting range is minimal, see Appendix D).

Therefore, both (7) and (8) can explain the behavior of the data for the *simulated* scales. In order to see whether they are useful to explain the experiments we consider the quantity $Z_c(T) = z(T, \xi_{\text{films}})T/T_c$, where $z(T, \xi_{\text{films}})$ is the derivative of either (7) or (8) at ξ_{films}. The result is plotted in Fig. 4 (see Appendix D for the full fit parameters). Remarkably, the convergent ansatz of (7) produces an almost constant Z_c in a wide T range, which additionally fits well the experimental value of $Z_c \approx 9.62$. The activated dynamics of (8), on the other hand, is not a good fit for the experimental behavior (inset to Fig. 4).

Using simulations for very large systems with many replicas on Janus II we have found that the growth of the SG coherence length is controlled by a time-dependent $z(T, \xi(t_w))$ exponent. After describing the dynamics as governed by a crossover between a critical and a low-temperature fixed point, we have been able to model this growth quantitatively and to extrapolate to experimental length scales. The resulting exponent is consistent with the most recent experimental measurements for power-law dynamics. In addition, we find clear evidence of non-coarsening dynamics at the experimental scale and find that temperatures $T \lesssim 0.7$ are free of critical effects and therefore safe for numerical studies of the SG phase.

An open question concerns the generality of these results. Indeed, CuMn is a Heisenberg, rather than Ising, SG. However, even the purest Heisenberg system has unavoidable anisotropies, such as Dzyaloshinsky-Moriya interactions [44]. These interactions, though tiny, extend over dozens of lattice spacings, which magnifies their effect. In fact, we know that Ising is the ruling universality
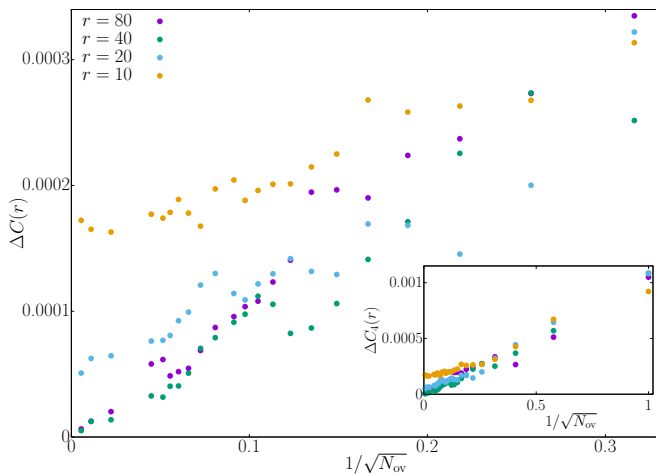
FIG. 5. Rapid reduction in the statistical error for the overlap autocorrelation function $C_4(T, r, t_w)$ with increasing number of replicas N_R. We plot $\Delta C(r)$ for $T = 0.7$ and $t_w = 2^{32}$ and several values of r as a function of the number of possible overlaps $[N_{ov} = N_R(N_R-1)/2]$. For large values of r the error is essentially linear in $1/N_R$. The inset shows the whole range from $N_R = 2$ (the minimum to define C_4), while the main plot is a close up of the large-N_R sector. The simulations reported in this paper have $N_R = 256$.

class in the presence of coupling anisotropies [45]. We also remark that high-quality measurements on GeMn are excellently fit with Ising scaling laws [7]. Our results also match the most recent and accurate measurements on CuMn [5].

More generally, this study is a clear demonstration of the importance of high-precision results for the investigation of glassiness. Indeed, reducing the errors has shown that the aging rate slows down during the dynamics, contrary to previous findings. A similar change of paradigm might happen for structural glasses.
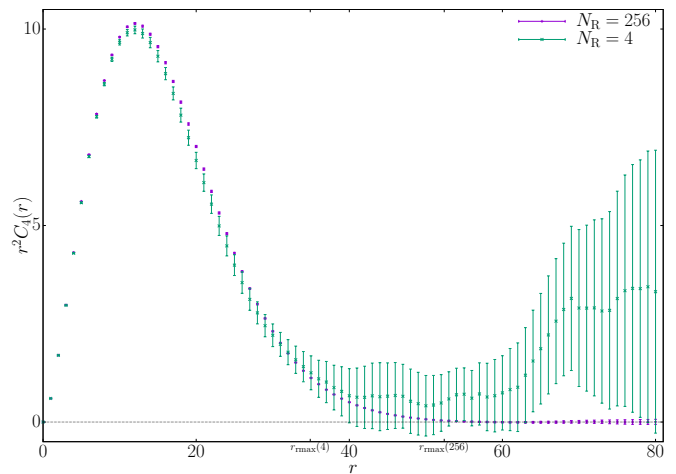
FIG. 6. Comparison of $r^2 C_4(r)$, function whose integral is used to estimate the coherence length, as computed with 4 and 256 replicas and the same number $N_S = 16$ of samples ($T = 0.7, t_w = 2^{34}$). We have marked on the x axis the resulting self-consistent cutoffs (see Appendix B) used to estimate the I_k integrals in both cases.

Appendix A: Error reduction for high number of replicas

As mentioned in the main paper, the choice of the number of replicas (N_R) and samples (N_S) was taken with the aim of improving the estimation of observables related to temperature chaos in future work, where it is important to maximize the number of possible overlaps (pairs of replicas) $N_{ov} = N_R(N_R - 1)/2$.

Unexpectedly, this has led to a dramatic increase in precision. Fig. 5 shows the reduction of the statistical error in the correlation function C_4 as a function of $1/\sqrt{N_{ov}}$. Moreover, this effect is enhanced as r increases, which leads to a qualitative improvement in the computation of the $I_k(T, r, t_w)$ integrals (Fig. 6).

Appendix B: Controlling finite-size effects

In order to obtain an estimate for $\xi_{k,k+1}(T, t_w) = I_{k+1}(T, t_w)/I_k(T, t_w)$ we need to compute the integrals

$$I_k(T, t_w) = \int_0^\infty dr\, r^k C_4(T, r, t_w). \quad (B1)$$

As discussed in [22], the main difficulty in this computation is handling the large-r tail where relative errors $[\Delta C_4(T, r, t_w)/C_4(T, r, t_w)]$ are big. We have to consider two issues: a) how to minimize the statistical errors and b) how to check for finite-size effects (which will appear when ξ/L becomes relatively large).

As explained in more detail in [22, 27], our estimate of $I_k(T, t_w)$ is the sum of the numerical integral of our measured $C_4(T, r, t_w)$ up to a self-consistent cutoff and a
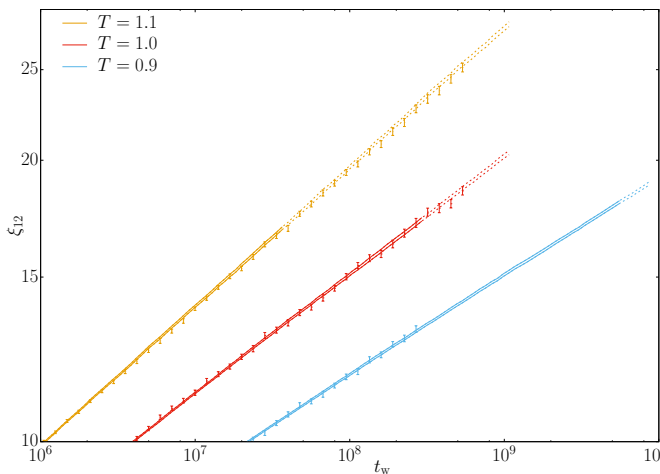
FIG. 7. Comparison between the $\xi_{12}(T, t_{\rm w})$ reported in this paper, computed in $L = 160$ lattices with $N_{\rm S} = 16$ samples and $N_{\rm R} = 256$ replicas, and that of [26] ($L = 256$; $N_{\rm S} = 50$; $N_{\rm R} = 4$ for $T = 0.9, 1.0$ and $N_{\rm R} = 8$ for $T = 1.1$). For the $L = 160$ simulations, we plot with two parallel lines the error interval for $\xi_{12}(T, t_{\rm w})$. Only the $t_{\rm w}$ range depicted with continuous lines is used in the paper, the extension with dashed lines represents the discarded times with $\xi_{12} > \xi_{12}^{\rm max}$ (see Table I). These curves were generated with the I_k^3 estimator for the integrals (B7). The values from the $L = 256$ simulations are plotted with conventional error bars. Notice that both curves are compatible even beyond this cutoff.

tail contribution estimated with a smooth extrapolating function $F(r) \sim r^{-\theta} f(r/\xi)$.

In short, the procedure is

1. Obtain $F(r)$ with fits of C_4 in a self-consistent region $[r_{\rm min}, r_{\rm max}]$ where the signal-to-noise ratio is still good.

2. Integrate C_4 numerically up to some cutoff and add the analytical integral of $F(r)$ beyond the cutoff to estimate the tail contribution.

There are several choices as to how to implement these steps, which we have used to control for systematic effects. For the extrapolating function $F(r)$, we consider first

$$F_1(r) = A_1 r^{-\theta} {\rm e}^{-(r/\xi)^{\beta_1}}. \tag{B2}$$

Where θ is the replicon exponent discussed in the text and we fit for A_1, β_1 and ξ. This analytical form is motivated by the fact that this is the simplest choice that avoids a pole singularity in the Fourier transform of $C_4(T, r, t_{\rm w})$ at finite $t_{\rm w}$. In order to check for finite-size effects we also consider a second function $F_2(r)$ resulting from fits that include the first-image term:

$$F_2^*(r) = A_2 \left[\frac{{\rm e}^{-(r/\xi)^{\beta_2}}}{r^\theta} + \frac{{\rm e}^{-((L-r)/\xi)^{\beta_2}}}{(L-r)^\theta} \right], \tag{B3}$$

T	0.55	0.625	0.7	0.8	0.9	1.0	1.1
$\xi_{\rm max}$	-	-	-	-	18.1	17.3	17

TABLE I. Cutoff values of $\xi_{12}^{\rm max}(T)$ below which we are guaranteed no finite-size effects in our $L = 160$ lattices. For $T < 0.9$ the growth of ξ_{12} is very slow and we never reach the cutoff value.

so we have a second extrapolating function

$$F_2(r) = A_2 r^{-\theta} {\rm e}^{-(r/\xi)^{\beta_2}}. \tag{B4}$$

For these fits we used $\theta = 0.35$. However, this value has very little effect on the final computation of $\xi_{k,k+1}$. We have checked this by recomputing the integrals with $\theta = 0$ and $\theta = 1 + \eta \approx 0.61$ (prediction of the droplet theory and influence of the $T = T_{\rm c}$ fixed point respectively). The different choices of θ led to a systematic effect smaller than 20% of the error bars in the worst case.

Once we have our two extrapolating functions F_1 and F_2 we can combine them with the C_4 data in several ways:

$$I_k^1 = \int_0^{r_{\rm max}} dr\; r^k C_4(T, r, t_{\rm w}) + \int_{r_{\rm max}}^\infty dr\; r^k F_1(r), \tag{B5}$$

$$I_k^2 = \int_0^{r_{\rm max}} dr\; r^k C_4(T, r, t_{\rm w}) + \int_{r_{\rm max}}^\infty dr\; r^k F_2(r), \tag{B6}$$

$$I_k^3 = \int_0^{r_{\rm min}} dr\; r^k C_4(T, r, t_{\rm w}) + \int_{r_{\rm min}}^\infty dr\; r^k F_2(r). \tag{B7}$$

The difference between I_k^2 and I_k^1 is always under 1 % in the error, so choosing between them has no effect in any computation. In contrast, I_k^1 and I_k^3 present measurable differences for long $t_{\rm w}$, at least for our highest temperatures, where the faster dynamics allows us to reach higher values of ξ_{12}/L. As a (very conservative) cutoff we have discarded all the $t_{\rm w}$ where $|I^1 - I^3|$ is larger than 20 % of the error bar, thus obtaining a $\xi_{12}^{\rm max}(T)$ below which we are assured not to have any finite-size effects in our $L = 160$ systems. The reader can find the values in table I.

As a final check that our data is not affected by finite-size effects, we have compared our $\xi_{12}(T, t_{\rm w})$ with that of [26]. This reference considers shorter simulations but with $L = 256$ and 50 samples. As shown in Fig. 7, the $L = 160$ and $L = 256$ data coincide even beyond our cutoff $\xi_{12}^{\rm max}$.

Appendix C: Josephson Crossover

In this section we will give additional details on the Josephson crossover which describes how $C_4(T, r, t_{\rm w})$ changes from being dominated by the $T = T_{\rm c}$ fixed point to being dominated by the $T = 0$ behavior as T and $t_{\rm w}$ vary. Assuming that $\xi(T, t_{\rm w}) \gg \ell_{\rm J}(T) \sim (T - T_{\rm c})^{-\nu}$, the
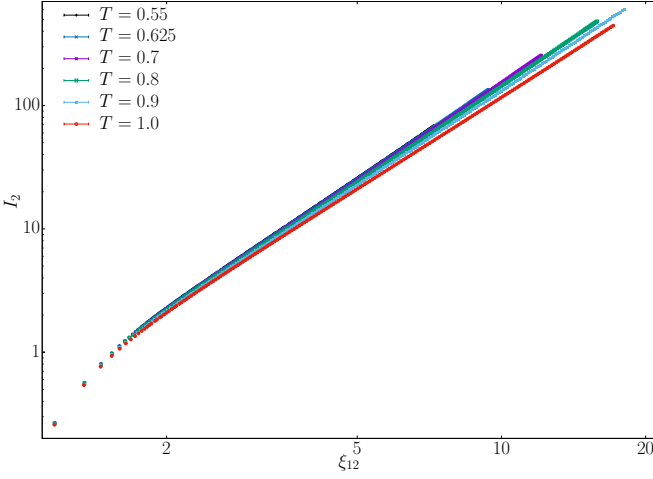
FIG. 8. Integral I_2 as a function of ξ_{12} in a logarithmic scale, for all our $T < T_c$ temperatures. We use the numerical derivative of this curve to compute the replicon exponent θ.
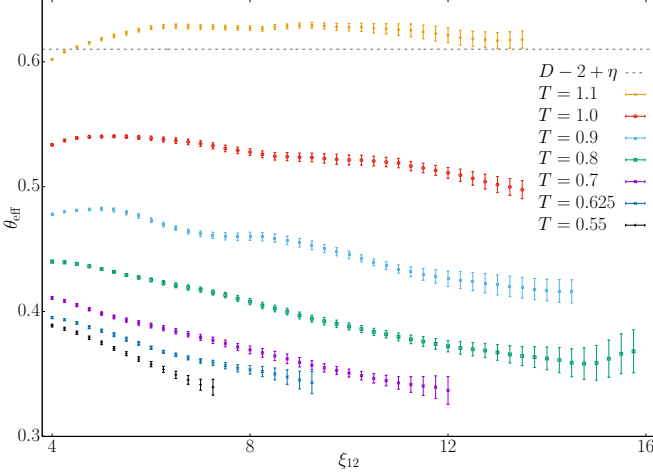

FIG. 9. Value of the replicon exponent $\theta(T, \xi_{12})$ computed from a numerical derivative of $\log I_2$ as a function of $\log \xi_{12}$, nicely illustrating the crossover between the $T = T_c$ and $T = 0$ fixed points.

crossover takes the form:

$$
C_4(T, r, t_w) \sim
\begin{cases}
\dfrac{1}{r^{D-2+\eta}}, & r \ll \ell_J(T), \\[2mm]
\dfrac{\ell_J^\theta}{\ell_J^{D-2+\eta}} \dfrac{1}{r^\theta} f_{\text{cutoff}}(r/\xi), & r \gg \ell_J(T).
\end{cases}
\tag{C1}
$$

In this equation, $f_{\text{cutoff}}(x)$ is an analytical function decaying as $\exp(-x^\beta)$. The prefactor for $\ell_J^\theta / \ell_J^{D-2+\eta}$ is fixed by the condition that the two asymptotic expansions connect smoothly at $r = \ell_J$. We arrive at an asymptotic expansion for the I_k integrals:

$$
I_k(T, \xi) = \frac{F_k}{\ell_J^{D-2+\eta}} \left(\frac{\xi}{\ell_J} \right)^{k+1-\theta} \left[1 + a_k \left(\frac{\xi}{\ell_J} \right)^{k+1-\theta} + \ldots \right],
\tag{C2}
$$

where F_k and a_k are amplitudes. Finally, we need to eliminate the unknown ξ in favor of the computable ξ_{12},

$$
\xi_{12}(T, \xi) = \frac{F_2}{F_1} \xi \left[1 + a_1' \left(\frac{\xi}{\ell_J} \right)^{2-\theta} + a_2 \left(\frac{\xi}{\ell_J} \right)^{3-\theta} + \ldots \right],
\tag{C3}
$$

where a_1' considers contributions both from the numerator $(-a_1)$ and from the denominator. The easiest way to obtain θ is to study the evolution of $\log I_2$ as a function of $\log \xi$. However, we have to settle for using $\log \xi_{12}$ as independent variable (see Fig. 8).

We can define an effective $\theta(T, \xi_{12})$ as

$$
\theta(T, \xi_{12}) = 3 - \frac{\mathrm{d} \log I_2(T, \xi_{12})}{\mathrm{d} \log \xi_{12}}
\tag{C4}
$$

$$
= \theta + b_2 \left(\frac{\xi_{12}}{\ell_J} \right)^{\theta-2} + b_3 \left(\frac{\xi_{12}}{\ell_J} \right)^{\theta-3} + \ldots .
\tag{C5}
$$

To estimate this derivative for a given ξ_{12}^*, we fit $\log I_2$ to a quadratic polynomial in $\log \xi_{12}$ in a $[0.75\xi_{12}^*, 1.25\xi_{12}^*]$ window. We then take the derivative of this polynomial at ξ^*. The procedure, as well as the wiggles in the resulting values of θ due to the extreme data correlation (see Fig. 9) may remind the reader of Fig. 1 in [8].

We have computed a fit to the first two terms in (C5) in the range $0 \leq \ell_J/\xi_{12} \leq 0.33$, resulting in the value of $\theta \approx 0.30$ reported in the main text.

The previous analysis solves the problem of the crossover between the $T = T_c$ and $T = 0$ fixed points. However, in the framework of the droplet picture one would also need to consider corrections to scaling at the $T = 0$ fixed point. This is precisely what the droplet fit in the main text to $\theta(x) \simeq Cx^\zeta$ does.

Appendix D: Parameter choices in our fits

We will discuss separately the choice of $\xi_{\min}$ for different temperatures and the choice of the value of ω.

1. Selection of $\xi_{12}^{\min}$ for each temperature

We have reported fits of our data to three different functional forms

$$
\log t_w = c_0(T) + c_1(T) \log \xi_{12} + c_2(T) \log^2 \xi_{12}, \tag{D1}
$$

$$
\log t_w = D(T) + z_\infty(T) \log \xi_{12} + E(T) \xi_{12}^{-\omega}, \tag{D2}
$$

$$
\log t_w = F(T) + z_c \log \xi_{12} + G(T) \xi_{12}^{\Psi}. \tag{D3}
$$

In these fits we have used $z_c = 6.69$ and $\omega = 0.35$ ($T < T_c$), $\omega = 1.12$ ($T = T_c$), as discussed in the main text. Full results for the fits to (D2) and (D3) can be seen in tables III and IV, for different fitting ranges. We include for both cases the extrapolated values of $z(T, \xi)$

for the experimental scale (as explained in the main text we use both $\xi_{12} = 38$ and $\xi_{12} = 76$) and for (D2) also the value of the $\xi \to \infty$ aging rate z_∞.

T	0.55	0.625	0.7	0.8	0.9	1.0	1.1
$\xi_{12}^{\min}$	4	5	6	8	8	9	5

TABLE II. Values of $\xi_{12}^{\min}(T)$ determining the common fitting range $\xi_{12} \geq \xi_{12}^{\min}$ for our three different fits of $\log t_{\mathrm{w}}$ as a function of $\log \xi_{12}$.

In order to make the choice of fitting range for the values plotted in the paper we have followed two criteria. Firstly we require the parameters of the fit to be stable inside the error when we increase $\xi_{12}^{\min}$. Secondly, we impose that $\xi_{\min}$ be monotonically increasing in T (with the exception of T_{c}, which has different behavior). Table II shows our final choices for $\xi_{12}^{\min}(T)$, which is the same for all three fits.

2. Selection of ω

For our most important result, namely the extrapolation of the aging rate to the experimental scale of $\xi_{12} = 38, 76$, we have repeated our fits with our upper and lower bounds for $\omega = \theta(\xi_{\mathrm{films}})$ (RSB and droplet extrapolations, respectively). The results are completely compatible, as we can see in table V.

[1] J. A. Mydosh, *Spin Glasses: an Experimental Introduction* (Taylor and Francis, London, 1993).

[2] A. P. Young, *Spin Glasses and Random Fields* (World Scientific, Singapore, 1998).

[3] E. Marinari, G. Parisi, F. Ricci-Tersenghi, J. J. Ruiz-Lorenzo, and F. Zuliani, J. Stat. Phys. **98**, 973 (2000), arXiv:cond-mat/9906076.

[4] Y. G. Joh, R. Orbach, G. G. Wood, J. Hammann, and E. Vincent, Phys. Rev. Lett. **82**, 438 (1999).

[5] Q. Zhai, D. C. Harrison, D. Tennant, E. D. Dalhberg, G. G. Kenning, and R. L. Orbach, Phys. Rev. B **95**, 054304 (2017).

[6] S. Guchhait and R. Orbach, Phys. Rev. Lett. **112**, 126401 (2014).

[7] S. Guchhait and R. L. Orbach, Phys. Rev. Lett. **118**, 157203 (2017).

[8] F. Belletti, M. Cotallo, A. Cruz, L. A. Fernandez, A. Gordillo-Guerrero, M. Guidetti, A. Maiorano, F. Mantovani, E. Marinari, V. Martín-Mayor, A. M. Sudupe, D. Navarro, G. Parisi, S. Perez-Gaviro, J. J. Ruiz-Lorenzo, S. F. Schifano, D. Sciretti, A. Tarancon, R. Tripiccione, J. L. Velasco, and D. Yllanes (Janus Collaboration), Phys. Rev. Lett. **101**, 157201 (2008), arXiv:0804.1471.

[9] M. Lulli, G. Parisi, and A. Pelissetto, Phys. Rev. E **93**, 032126 (2016).

[10] F. Belletti, M. Guidetti, A. Maiorano, F. Mantovani, S. F. Schifano, R. Tripiccione, M. Cotallo, S. Perez-Gaviro, D. Sciretti, J. L. Velasco, A. Cruz, D. Navarro, A. Tarancon, L. A. Fernandez, V. Martín-Mayor, A. Muñoz-Sudupe, D. Yllanes, A. Gordillo-Guerrero, J. J. Ruiz-Lorenzo, E. Marinari, G. Parisi, M. Rossi, and G. Zanier (Janus Collaboration), Computing in Science and Engineering **11**, 48 (2009).

[11] M. Baity-Jesi, R. A. Baños, A. Cruz, L. A. Fernandez, J. M. Gil-Narvion, A. Gordillo-Guerrero, M. Guidetti, D. Iniguez, A. Maiorano, F. Mantovani, E. Marinari, V. Martín-Mayor, J. Monforte-Garcia, A. Munoz Sudupe, D. Navarro, G. Parisi, M. Pivanti, S. Perez-Gaviro, F. Ricci-Tersenghi, J. J. Ruiz-Lorenzo, S. F. Schifano, B. Seoane, A. Tarancon, P. Tellez, R. Tripiccione, and D. Yllanes, Eur. Phys. J. Special Topics **210**, 33 (2012), arXiv:1204.4134.

[12] M. Baity-Jesi, R. A. Baños, A. Cruz, L. A. Fernandez, J. M. Gil-Narvion, A. Gordillo-Guerrero, D. Iniguez, A. Maiorano, F. Mantovani, E. Marinari, V. Martín-Mayor, J. Monforte-Garcia, A. Muñoz Sudupe, D. Navarro, G. Parisi, S. Perez-Gaviro, M. Pivanti, F. Ricci-Tersenghi, J. J. Ruiz-Lorenzo, S. F. Schifano, B. Seoane, A. Tarancon, R. Tripiccione, and D. Yllanes (Janus Collaboration), Comp. Phys. Comm **185**, 550 (2014), arXiv:1310.1032.

[13] M. Baity-Jesi, E. Calore, A. Cruz, L. A. Fernandez, J. M. Gil-Narvión, A. Gordillo-Guerrero, D. Iñiguez, A. Maiorano, E. Marinari, V. Martin-Mayor, J. Monforte-Garcia, A. Muñoz Sudupe, D. Navarro, G. Parisi, S. Perez-Gaviro, F. Ricci-Tersenghi, J. J. Ruiz-Lorenzo, S. F. Schifano, B. Seoane, A. Tarancón, R. Tripiccione, and D. Yllanes, Proceedings of the National Academy of Sciences **114**, 1838 (2017).

[14] R. Alvarez Baños, A. Cruz, L. A. Fernandez, J. M. Gil-Narvion, A. Gordillo-Guerrero, M. Guidetti, A. Maiorano, F. Mantovani, E. Marinari, V. Martín-Mayor, J. Monforte-Garcia, A. Muñoz Sudupe, D. Navarro, G. Parisi, S. Perez-Gaviro, J. J. Ruiz-Lorenzo, S. F. Schifano, B. Seoane, A. Tarancon, R. Tripiccione, and D. Yllanes (Janus Collaboration), J. Stat. Mech. **2010**, P06026 (2010), arXiv:1003.2569.

[15] R. Alvarez Baños, A. Cruz, L. A. Fernandez, J. M. Gil-Narvion, A. Gordillo-Guerrero, M. Guidetti, A. Maiorano, F. Mantovani, E. Marinari, V. Martín-Mayor, J. Monforte-Garcia, A. Muñoz Sudupe, D. Navarro, G. Parisi, S. Perez-Gaviro, J. J. Ruiz-Lorenzo, S. F. Schifano, B. Seoane, A. Tarancon, R. Tripiccione, and D. Yllanes (Janus Collaboration), Phys. Rev. Lett. **105**, 177202 (2010), arXiv:1003.2943.

[16] M. Baity-Jesi, E. Calore, A. Cruz, L. A. Fernandez, J. M. Gil-Narvion, A. Gordillo-Guerrero, D. Iñiguez, A. Maio-

rano, E. Marinari, V. Martin-Mayor, J. Monforte-Garcia, A. Muñoz Sudupe, D. Navarro, G. Parisi, S. Perez-Gaviro, F. Ricci-Tersenghi, J. J. Ruiz-Lorenzo, S. F. Schifano, B. Seoane, A. Tarancon, R. Tripiccione, and D. Yllanes (Janus Collaboration), Phys. Rev. Lett. **118**, 157202 (2017).

[17] W. Wang, J. Machta, H. Munoz-Bauza, and H. G. Katzgraber, Phys. Rev. B **96**, 184417 (2017).

[18] S. F. Edwards and P. W. Anderson, Journal of Physics F: Metal Physics **5**, 965 (1975).

[19] M. Baity-Jesi, R. A. Baños, A. Cruz, L. A. Fernandez, J. M. Gil-Narvion, A. Gordillo-Guerrero, D. Iniguez, A. Maiorano, F. Mantovani, E. Marinari, V. Martín-Mayor, J. Monforte-Garcia, A. Muñoz Sudupe, D. Navarro, G. Parisi, S. Perez-Gaviro, M. Pivanti, F. Ricci-Tersenghi, J. J. Ruiz-Lorenzo, S. F. Schifano, B. Seoane, A. Tarancon, R. Tripiccione, and D. Yllanes (Janus Collaboration), Phys. Rev. B **88**, 224416 (2013), arXiv:1310.2910.

[20] D. J. Amit and V. Martín-Mayor, *Field Theory, the Renormalization Group and Critical Phenomena*, 3rd ed. (World Scientific, Singapore, 2005).

[21] D. Yllanes, *Rugged Free-Energy Landscapes in Disordered Spin Systems*, Ph.D. thesis, Universidad Complutense de Madrid (2011), arXiv:1111.0266.

[22] F. Belletti, A. Cruz, L. A. Fernandez, A. Gordillo-Guerrero, M. Guidetti, A. Maiorano, F. Mantovani, E. Marinari, V. Martín-Mayor, J. Monforte, A. Muñoz Sudupe, D. Navarro, G. Parisi, S. Perez-Gaviro, J. J. Ruiz-Lorenzo, S. F. Schifano, D. Sciretti, A. Tarancon, R. Tripiccione, and D. Yllanes (Janus Collaboration), J. Stat. Phys. **135**, 1121 (2009), arXiv:0811.2864.

[23] Janus Collaboration, (in preparation).

[24] L. Berthier, P. Charbonneau, Y. Jin, G. Parisi, B. Seoane, and F. Zamponi, Proc. Natl. Acad. Sci. USA **113**, 8397 (2016).

[25] B. Seoane and F. Zamponi, Soft Matter (2018, in press), 10.1039/C8SM00859K.

[26] L. A. Fernández and V. Martín-Mayor, Phys. Rev. B **91**, 174202 (2015).

[27] L. A. Fernández, E. Marinari, V. Martín-Mayor, G. Parisi, and J. Ruiz-Lorenzo, "An experiment-oriented analysis of 2d spin-glass dynamics: a twelve time-decades scaling study," (2018), submitted, arXiv:1805.06738.

[28] Our result $z_c = z(T = T_c) = 6.69(6)$ is significantly more accurate that $z_c = 6.80(15)$ [9] and $z_c = 6.86(16)$ [8], even though, unlike Ref. [8], we allow for corrections to scaling, which increases the statistical error, see Appendix D.

[29] A naive explanation for the curvature in $\xi_{12}(T, t_w)$ would be the existence of finite-size effects (see [8]). However, c_2 grows as we decrease T, while finite-size effects would be controlled by ξ_{12}/L, which is smaller for the lower temperatures. See Appendix B for extensive checks that our $L = 160$ are safe.

[30] W. L. McMillan, Phys. Rev. B **28**, 5216 (1983).

[31] A. J. Bray and M. A. Moore, Phys. Rev. Lett. **41**, 1068 (1978).

[32] D. S. Fisher and D. A. Huse, Phys. Rev. Lett. **56**, 1601 (1986).

[33] B. D. Josephson, Phys. Lett. **21**, 608 (1966).

[34] In theory, $\ell_J \propto [1 + j_0(T_c - T)^\nu + j_1(T_c - T)^{\omega\nu}](T_c - T)^{-\nu}$, where we include analytic (j_0) and confluent (j_1) scaling corrections with $\omega = 1.12(10)$ [19]. For Fig. 3, we have chosen j_0 and j_1 to obtain the best collapse for the lowest temperatures.

[35] S. Boettcher, Eur. Phys. J. B **38**, 83 (2004), arXiv:cond-mat/0310698.

[36] J.-P. Bouchaud, V. Dupuis, J. Hammann, and E. Vincent, Phys. Rev. B **65**, 024439 (2001).

[37] L. Berthier and J.-P. Bouchaud, Phys. Rev. B **66**, 054404 (2002).

[38] A. G. Schins, A. F. M. Arts, and H. W. de Wijn, Phys. Rev. Lett. **70**, 2340 (1993).

[39] H. Rieger, J. Phys. A **26**, L615 (1993).

[40] $G(T)$ in (8) goes to zero at T_c as $(T_c - T)^{\Psi\nu}$, which is another form of the Josephson scaling.

[41] A. Billoire and E. Marinari, Journal of Physics A: Mathematical and General **34**, L727 (2001).

[42] G. Rogers and M. A. Moore, J. Phys. A: Math. Gen. **22**, 1085 (1989).

[43] S. G. W. Colborne, J. Phys. A: Math. Gen. **23**, 4013 (1990).

[44] A. J. Bray and M. A. Moore, J. Phys. C: Solid St. Phys. **15**, 3897 (1982).

[45] M. Baity-Jesi, L. A. Fernandez, V. Martín-Mayor, and J. M. Sanz, Phys. Rev. **89**, 014202 (2014), arXiv:1309.1599.

		$\xi_{\min}=3.5$	$\xi_{\min}=4$	$\xi_{\min}=5$	$\xi_{\min}=6$	$\xi_{\min}=7$	$\xi_{\min}=8$	$\xi_{\min}=9$
$T=0.55$	z_∞	23.61(28)	**24.22(40)**	25.30(86)	22.9(31)			
	$z(\xi\!=\!38)$	19.49(15)	**19.80(20)**	20.32(41)	19.2(14)			
	$z(\xi\!=\!76)$	20.38(18)	**20.75(24)**	21.39(51)	20.0(18)			
	χ^2/dof	40(17)/133	**10.2(54)/111**	3.0(12)/73	1.71(76)/40			
$T=0.625$	z_∞	19.85(17)	20.26(23)	**20.60(41)**	20.16(84)			
	$z(\xi\!=\!38)$	16.538(91)	16.74(12)	**16.90(19)**	16.71(37)			
	$z(\xi\!=\!76)$	17.25(11)	17.50(14)	**17.69(24)**	17.45(47)			
	χ^2/dof	81(34)/167	18(10)/147	**8.3(21)/114**	5.1(19)/86			
$T=0.7$	z_∞	17.04(18)	17.23(21)	17.61(27)	**18.23(35)**	18.63(62)		
	$z(\xi\!=\!38)$	14.295(88)	14.38(11)	14.55(13)	**14.81(15)**	14.96(25)		
	$z(\xi\!=\!76)$	14.89(11)	15.00(13)	15.21(16)	**15.54(19)**	15.75(32)		
	χ^2/dof	116(40)/190	66(36)/173	33(24)/144	**9.3(84)/119**	4.9(21)/98		
$T=0.8$	z_∞	13.76(15)	14.06(19)	14.53(26)	15.19(35)	15.68(42)	**16.18(58)**	16.55(78)
	$z(\xi\!=\!38)$	11.787(73)	11.921(89)	12.11(12)	12.37(15)	12.55(17)	**12.73(22)**	12.85(28)
	$z(\xi\!=\!76)$	12.211(93)	12.38(11)	12.63(15)	12.98(19)	13.23(23)	**13.47(30)**	13.65(39)
	χ^2/dof	351(104)/185	188(72)/170	93(41)/146	27(16)/125	12.4(82)/107	**6.2(31)/91**	4.9(21)/77
$T=0.9$	z_∞	11.00(13)	11.29(18)	11.54(24)	11.80(31)	12.55(41)	**13.16(68)**	12.3(13)
	$z(\xi\!=\!38)$	9.748(65)	9.883(93)	9.98(11)	10.08(13)	10.34(16)	**10.55(25)**	10.33(41)
	$z(\xi\!=\!76)$	10.017(82)	10.18(11)	10.32(14)	10.45(17)	10.82(21)	**11.11(34)**	10.80(60)
	χ^2/dof	310(150)/165	129(64)/152	79(44)/131	63(35)/113	22(13)/98	**5.9(21)/84**	6.4(79)/72
$T=1.0$	z_∞	8.60(11)	8.69(15)	8.83(20)	8.97(53)	9.29(45)	9.36(46)	**10.28(89)**
	$z(\xi\!=\!38)$	8.041(59)	8.080(73)	8.132(93)	8.21(22)	8.27(18)	8.34(17)	**8.63(32)**
	$z(\xi\!=\!76)$	8.162(74)	8.210(86)	8.28(11)	8.38(29)	8.46(24)	8.57(24)	**8.98(44)**
	χ^2/dof	43(30)/137	27(18)/126	16(13)/107	12(25)/91	10.4(91)/78	8.4(60)/66	**2.9(21)/55**
$T=1.1$	z_∞	6.672(44)	6.671(41)	**6.689(63)**	6.751(84)	6.80(12)	7.00(18)	7.02(21)
	$z(\xi\!=\!38)$	6.682(32)	6.673(41)	**6.694(50)**	6.732(68)	6.77(10)	6.92(14)	6.94(16)
	$z(\xi\!=\!76)$	6.677(33)	6.671(41)	**6.691(54)**	6.742(72)	6.79(11)	6.96(16)	6.99(16)
	χ^2/dof	32(19)/119	31(20)/109	**26(16)/92**	19(10)/78	16.8(74)/66	5.9(20)/55	6.3(27)/46

TABLE III. Parameters of the fits to (D2) for different fitting ranges $\xi_{12} \geq \xi_{12}^{\min}$. We use $\omega = 0.35$ ($\omega = 1.12$ for $T = T_\mathrm{c}$). The fitting range that we choose for our final values is highlighted in boldface.

		$\xi_{\min}=3.5$	$\xi_{\min}=4$	$\xi_{\min}=5$	$\xi_{\min}=6$	$\xi_{\min}=7$	$\xi_{\min}=8$	$\xi_{\min}=9$
$T=0.55$	$z(\xi=38)$	24.07(41)	**24.25(55)**	24.6(11)	24.7(81)			
	$z(\xi=76)$	28.86(69)	**29.18(95)**	29.9(19)	30(15)			
	$B(T)$	13.78(65)	**13.45(92)**	12.8(18)	18(13)			
	Ψ	0.3512(92)	**0.355(21)**	0.372(33)	0.29(24)			
	χ^2/dof	13.3(47)/133	**6.8(20)/111**	3.2(15)/73	1.7(27)/40			
$T=0.625$	$z(\xi=38)$	19.73(22)	19.72(28)	**19.36(45)**	18.53(77)			
	$z(\xi=76)$	23.33(38)	23.31(49)	**22.66(79)**	21.1(13)			
	$B(T)$	10.36(37)	10.39(52)	**11.3(11)**	14.0(30)			
	Ψ	0.354(14)	0.352(12)	**0.334(21)**	0.290(39)			
	χ^2/dof	19(10)/167	15(10)/147	**8.5(33)/114**	4.5(14)/86			
$T=0.7$	$z(\xi=38)$	16.58(22)	16.44(23)	16.35(27)	**16.51(32)**	16.55(52)		
	$z(\xi=76)$	19.40(37)	19.14(40)	18.98(47)	**19.29(58)**	19.4(10)		
	$B(T)$	7.32(34)	7.63(43)	7.84(59)	**7.41(75)**	7.3(14)		
	Ψ	0.364(13)	0.354(12)	0.354(24)	**0.358(23)**	0.360(39)		
	χ^2/dof	49(38)/190	28(20)/173	10.5(83)/144	**6.3(31)/119**	5.7(29)/98		
$T=0.8$	$z(\xi=38)$	13.37(18)	13.39(21)	13.45(25)	13.68(31)	13.80(35)	**13.94(45)**	14.1(17)
	$z(\xi=76)$	15.44(33)	15.48(37)	15.60(46)	16.06(59)	16.31(68)	**16.59(93)**	17.1(38)
	$B(T)$	4.16(25)	4.13(29)	4.01(38)	3.57(43)	3.36(48)	**3.13(66)**	3.0(19)
	Ψ	0.392(13)	0.390(19)	0.395(18)	0.421(27)	0.443(31)	**0.447(50)**	0.46(18)
	χ^2/dof	31(19)/185	29(19)/170	22(17)/146	10.0(60)/125	7.5(34)/107	**5.5(21)/91**	5(11)/77
$T=0.9$	$z(\xi=38)$	10.76(17)	10.86(21)	10.82(24)	10.86(27)	11.23(35)	**11.49(54)**	11.13(56)
	$z(\xi=76)$	12.12(30)	12.31(39)	12.24(45)	12.31(53)	13.12(73)	**13.7(12)**	12.9(12)
	$B(T)$	2.15(19)	2.01(23)	2.07(31)	2.00(39)	1.52(31)	**1.18(45)**	1.67(77)
	Ψ	0.417(23)	0.430(34)	0.431(28)	0.427(41)	0.490(51)	**0.546(88)**	0.47(10)
	χ^2/dof	68(44)/165	46(25)/152	41(25)/131	38(24)/113	17(10)/98	**8.7(45)/84**	4.8(25)/72
$T=1.0$	$z(\xi=38)$	8.53(15)	8.54(18)	8.55(20)	8.56(30)	8.59(60)	8.74(72)	**9.22(18)**
	$z(\xi=76)$	9.19(27)	9.20(33)	9.22(39)	9.25(58)	9.3(12)	9.7(16)	**10.9(45)**
	$B(T)$	0.85(14)	0.84(18)	0.83(22)	0.79(40)	0.7(10)	0.5(10)	**1.4(19)**
	Ψ	0.440(36)	0.441(51)	0.444(64)	0.45(10)	0.49(25)	0.55(30)	**0.34(71)**
	χ^2/dof	12.6(95)/137	12.1(90)/126	10.0(87)/107	9.3(83)/91	8.2(97)/78	07(11)/66	**11(11)/55**
$T=1.1$	$z(\xi=38)$	6.684(12)	6.682(14)	**6.684(11)**	6.672(31)	6.683(32)	6.694(31)	6.712(41)
	$z(\xi=76)$	6.684(13)	6.681(11)	**6.682(14)**	6.674(41)	6.684(41)	6.692(31)	6.721(42)
	$B(T)$	1.9(10)	1.71(91)	**0.4(27)**	0.02(64)	0.0(26)	1.5(26)	1.2(10)
	Ψ	-0.0030(49)	0.0037(68)	**0.03(15)**	0.29(42)	0.37(55)	0.002(16)	0.023(51)
	χ^2/dof	34(20)/119	33(19)/109	**27(18)/92**	25(18)/78	23(15)/66	21(14)/55	11.0(26)/46

TABLE IV. Parameters of the fits to (D3) for different fitting ranges $\xi_{12} \geq \xi_{12}^{\min}$. We use $z_{\mathrm{c}} = 6.69$. The fitting range that we choose for our final values is highlighted in boldface.

	$z(T, \xi_{12} = 38)$		$z(T, \xi_{12} = 76)$	
	$\omega = 0.35$	$\omega = 0.28$	$\omega = 0.35$	$\omega = 0.25$
$T = 0.55$	19.80(20)	20.08(22)	20.75(24)	21.41(27)
$T = 0.625$	16.90(19)	17.07(20)	17.69(24)	18.13(27)
$T = 0.7$	14.81(15)	14.93(16)	15.54(19)	15.87(21)
$T = 0.8$	12.73(22)	12.81(23)	13.47(30)	13.71(32)
$T = 0.9$	10.55(25)	10.61(26)	11.11(34)	11.28(37)
$T = 1.0$	8.63(32)	8.68(33)	8.98(44)	9.02(42)

TABLE V. Comparison of our estimates of the experimental aging rate $z(T, \xi_{12} = \xi_{\text{films}})$ for $\xi_{\text{films}} = 38$ and $\xi_{\text{films}} = 76$ using our lower and upper bounds for $\omega = \theta(\xi_{\text{films}})$. The choice of ω is immaterial, since even in the worst case (lowest temperatures for $\xi_{\text{films}} = 76$) there is only a two-sigma difference.